MIT Open Access Articles

# Photonic Platforms Using In#Plane Optical Anisotropy of Tin (II) Selenide and Black Phosphorus

The MIT Faculty has made this article openly available. ***Please share*** how this access benefits you. Your story matters.

| | |
|---|---|
| **Citation** | Jo, Seong Soon, Wu, Changming, Zhu, Linghan, Yang, Li, Li, Mo et al. 2021. "Photonic Platforms Using In#Plane Optical Anisotropy of Tin (II) Selenide and Black Phosphorus." Advanced Photonics Research, 2 (12). |
| **As Published** | 10.1002/ADPR.202100176 |
| **Publisher** | Wiley |
| **Version** | Final published version |
| **Citable link** | https://hdl.handle.net/1721.1/139809 |
| **Terms of Use** | Creative Commons Attribution 4.0 International license |
| **Detailed Terms** | https://creativecommons.org/licenses/by/4.0/ |

Massachusetts Institute of Technology

DSpace@MIT

ADVANCED PHOTONICS RESEARCH Open Access
www.adpr-journal.com

# Photonic Platforms Using In-Plane Optical Anisotropy of Tin (II) Selenide and Black Phosphorus

*Seong Soon Jo, Changming Wu, Linghan Zhu, Li Yang, Mo Li, and Rafael Jaramillo**

**Among layered and 2D semiconductors, there are many with substantial optical anisotropy within individual layers, including group-IV monochalcogenides *MX* (*M* = Ge or Sn and *X* = S or Se) and black phosphorous (bP). Recent work has suggested that the in-plane crystal orientation in such materials can be switched (e.g., rotated through 90°) through an ultrafast, displacive (i.e., nondiffusive), nonthermal, and lower-power mechanism by strong electric fields, due to in-plane dielectric anisotropy. In theory, this represents a new mechanism for light-controlling-light in photonic integrated circuits (PICs). Herein, numerical device modeling is used to study device concepts based on switching the crystal orientation of SnSe and bP in PICs. Ring resonators and 1 × 2 switches with resonant conditions that change with the in-plane crystal orientations SnSe and bP are simulated. The results are broadly applicable to 2D materials with ferroelectric and ferroelastic crystal structures including SnO, GeS, and GeSe.**

## 1. Introduction

Layered and 2D semiconductors interact strongly with light and feature a variety of crystalline structures that, at least in principle, can be switched quickly and with low energy input. This suggests a variety of applications of 2D materials for active optical phase modulation in photonic integrated circuits (PICs). Many 2D semiconductors feature bandgaps in the range of 1–2 eV and therefore are favorable for refractive near-infrared (NIR) applications.[1] All layered materials are strongly birefringent, with refractive index much higher for electric field polarization within the layers (ordinary) than perpendicular (extraordinary).[2,3] Here, we focus on 2D materials that are substantially triaxial, with low optical symmetry within individual layers.[4,5] Among layered and 2D materials, there are many with substantial optical anisotropy within individual layers, including the group-IV monochalcogenides MX (M = Ge or Sn and X = S or Se) and black phosphorous (bP). We study whether the optical anisotropy within individual layers can be used to switch light in PIC devices, provided that a mechanism is available to switch the crystal orientation (i.e., the domain pattern). We use numerical device modeling to study how confined light interacts with these layered materials with varying crystal orientations and simulate several device concepts. Our results may be broadly applicable to 2D materials with ferroelectric and ferroelastic crystal structures (**Table 1**).

Our work is inspired by a theoretical prediction of nonthermal transformations between crystalline domains in ferroelastic 2D materials driven by light and in-plane dielectric anisotropy.[6–8] In **Figure 1**a, we illustrate energetically-degenerate ferroelastic domains in monolayer tin (II) selenide (SnSe). The structure has a rectangular unit cell, with lattice constants $a = 4.275$ $\AA$ (zigzag [ZZ] direction) and $b = 4.401\AA$ (armchair [AC] direction). The predicted switching effect is due to the substantial in-plane anisotropy of the dielectric tensor $\varepsilon_{ij}$. The dielectric energy for an applied electric field $\underline{E}$ depends on the polarization, and this polarization dependence generates a torque on the crystal. For sufficiently-strong electric field and dielectric anisotropy, theory predicts a barrierless transformation between ferroelastic domain types.[6] For materials that are ferroelectric and ferroelastic, both terms linear in $\underline{E}$ (i.e., ferroelectric polarization) and quadratic in $\underline{E}$ (i.e., dielectric polarization) may contribute to this effect. However, the linear term only responds to the low-frequency applied electric field, for which the crystal structure can follow the phase of the applied field. For high-frequency applied electric field, appropriate for switching triggered by optical pulses (i.e., light-controls-light), only the dielectric energy $\varepsilon_{ij}E_iE_j$ remains. Therefore, this effect is general for materials with anisotropic dielectric tensors. Theory predicts optomechanical switching occurring on a timescale of picoseconds, with

S. S. Jo, R. Jaramillo
Department of Materials Science and Engineering
Massachusetts Institute of Technology
Cambridge, MA 02139, USA
E-mail: rjaramil@mit.edu

C. Wu, M. Li
Department of Electrical and Computer Engineering
University of Washington
Seattle, WA 98195, USA

L. Zhu, L. Yang
Department of Physics
Washington University in St. Louis
St. Louis, MO 63130, USA

L. Yang
Institute of Materials Science and Engineering
Washington University in St. Louis
St. Louis, MO 63130, USA

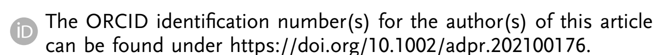
The ORCID identification number(s) for the author(s) of this article can be found under https://doi.org/10.1002/adpr.202100176.

© 2021 The Authors. Advanced Photonics Research published by Wiley-VCH GmbH. This is an open access article under the terms of the Creative Commons Attribution License, which permits use, distribution and reproduction in any medium, provided the original work is properly cited.

**DOI: 10.1002/adpr.202100176**

**Table 1.** Selection of layered and 2D materials with substantial optical anisotropy within individual layers. In this work, we consider devices using SnSe and bP; our results suggest similar applications of other materials.

| Material | *a* [Å] | *b* [Å] | Space group | Reference |
|---|---|---|---|---|
| SnO | 3.66 | 4.03 | $P_{mmn}$ | Zhou et al.[6] |
| SnSe | 4.28 | 4.40 | $P_{m2_1n}$ | Zhou et al.[6] |
| SnS | 4.08 | 4.31 | $P_{m2_1n}$ | Xiong et al.[27] |
| GeSe | 3.59 | 5.73 | $P_{m2_1n}$ | Zhou et al.[28] |
| GeS | 3.64 | 4.52 | $P_{m2_1n}$ | Xiong et al.[27] |
| bP | 3.30 | 4.63 | $P_{mna}$ | Wei et al.[29] |

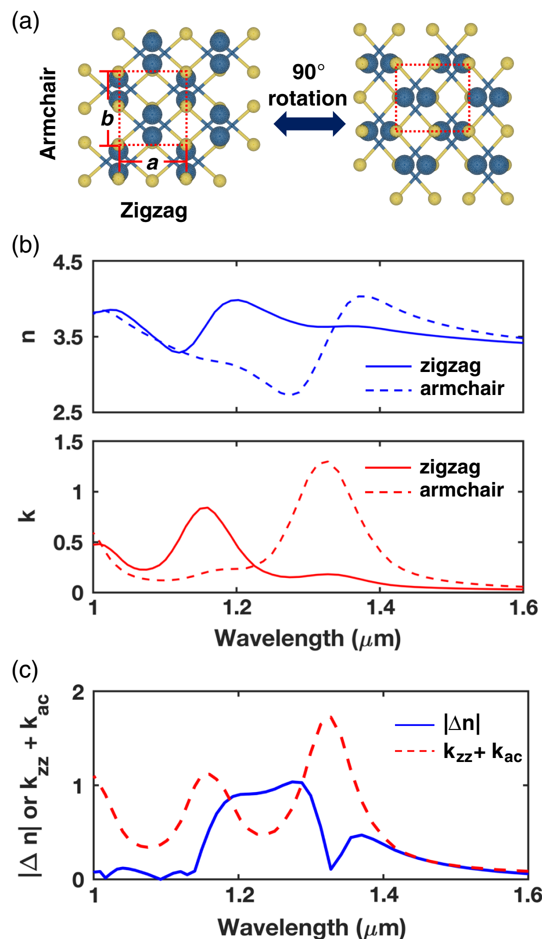


**Figure 1.** In-plane optical anisotropy for monolayer SnSe. a) Top view of SnSe crystal structure showing the rectangular 2D unit cell with ZZ (short axis) and AC (long axis) directions. b) Complex refractive index of monolayer SnSe for electric field polarized along the ZZ and AC directions, predicted by theory.[6] Theory underestimates the bandgap, which is in fact at 1.6 eV. Therefore, in real monolayer SnSe, the loss peaks (here seen in the NIR) would occur below 800 nm. c) Difference $|\Delta n| = |n_{zz} - n_{ac}|$ and sum $k_{zz} + k_{ac}$.

optical energy input on the scale of 0.001 aJ nm$^{-3}$.[6] Therefore, this optomechanical effect may be competitive for photonic modulators operating at a high bandwidth and with low power consumption.

Here we study devices based on switching ferroelastic domains in SnSe and bP and operating in the NIR and short-wavelength infrared (SWIR). The bandgap ($E_g$) of SnSe in bulk and monolayer forms is 0.9 and 1.6 eV, respectively, and is indirect in both cases.[9] For bP, $E_g$ is 0.3 and 2 eV for bulk and monolayer forms and is direct in both cases.[10] Optical anisotropy is enhanced below but near absorption resonances, so we design our devices to operate near $E_g$.[6] The complex dielectric tensors for SnSe and bP in bulk and monolayer forms are not well established experimentally. Therefore, for consistency throughout this work, we use refractive index data predicted by density functional theory (DFT). DFT has well-known systematic errors in predicting the energy of excited states, often resulting in underestimation of $E_g$. However, the predicted complex dielectric response is more accurate than excited-state energies because DFT produces accurate solutions for electron crystal wave functions, which are used to calculate the dielectric response in the random phase approximation (RPA).[11] In other words, DFT-predicted $n(\lambda)$ and $k(\lambda)$ data are often inaccurate in the abscissa but acceptable in the ordinate: the features associated with band-to-band transitions (such as the SnSe absorption resonances between 1 and 1.4 μm in Figure 1b) may rigidly shift along the energy (horizontal) axis to match the experiment.[12] In this work, the optical properties of SnSe are as calculated by DFT, and our simulated devices operate near DFT-predicted absorption resonances. Real devices will likely be designed to operate at higher photon energy, below but near the experimental $E_g$. The calculated optical properties for bP used here include a bandgap correction, and therefore the operating photon energy range for the simulated bP devices is more accurate than that for the simulated SnSe devices.

We study the usefulness of the optical anisotropy of layered materials with ferroelastic domains; we do not consider the mechanism of switching between domains, as we and others did in earlier work.[6–8] Both optical phase control and the domain switching mechanism rely on the anisotropic dielectric tensor. When an optical pulse in the visible–NIR is used for domain switching, only the electronic contribution to the dielectric response ($\varepsilon_{ij}^{\text{elec}}$, sometimes referred to as the optical dielectric constant, or $\varepsilon_\infty$) is important. The anisotropy of the dielectric response of triaxial layered and 2D materials is often enhanced at low frequency; for instance, for SnS, $\varepsilon_{ij}$ at low frequency is predicted to vary between 35 and 52 (values normalized to the susceptibility of free space) with varying electric field polarization within the layers.[13] In principle, low-frequency dielectric anisotropy could allow domain switching by direct-current electric fields, but in practice the required field strengths are attainable only with laser fields.

## 2. Properties of and Devices Based on SnSe

SnSe is a layered material, but has relatively high exfoliation energy, and as a result has not been widely studied in monolayer form.[14–16] Therefore, we use the published, theoretically-predicted complex refractive index of monolayer SnSe in our device


© 2021 The Authors. Advanced Photonics Research published by Wiley-VCH GmbH

simulations.[6] We show in Figure 1b the real ($n$) and imaginary ($k$) refractive indices along the ZZ and AC directions, and in Figure 1c, the difference $|\Delta n| = |n_{zz} - n_{ac}|$ and the sum $\sum k = k_{zz} + k_{ac}$ between these directions. We define a figure of merit FoM $= |\Delta n|/\sum k$ to capture the usefulness of ferroelastic domain switching for controlling optical phase with low loss. For monolayer SnSe, a maximum FoM of $\approx 2$ is achieved at wavelength $\lambda = 1.24\,\mu m$, at which $|\Delta n| = 0.93$ and $\sum k = 0.47$; see Figure S1, Supporting Information.[6] For reference, the widely studied phase-change material $Ge_2Sb_2Te_5$ exhibits $|n_c - n_a| \approx 2.7$ and $k_c + k_a \approx 2.1$ in the range $1.2 - 1.6\,\mu m$.[17–19] We note that the expression $|\Delta n|/|\Delta k|$ often appears in the literature as a FoM for phase-change materials for photonics. This is particularly useful for proposed applications that use optical absorption in one of the states, such as switchable attenuators. However, it can mislead for designing low-insertion-loss devices, because it can obscure optical loss. According to this definition, ferroelastic switching in monolayer SnSe has a FoM of 152.

We use the optical properties of monolayer SnSe to simulate an optical switch based on a silicon nitride ($Si_3N_4$) ring resonator integrated with a patch of monolayer SnSe that can switch between different ferroelastic domains (**Figure 2**a). The $Si_3N_4$ waveguide has width and thickness of 1 μm and 0.22 μm, respectively, and the SnSe layer thickness is 9 Å. The ring resonator has a bending radius of 50 μm and a realistic quality factor ($Q$) of $2 \times 10^5$.[20,21] The guided optical modes couple evanescently to the SnSe monolayer. One principal axis of the monolayer SnSe (ZZ or AC) is aligned with the direction of light propagation ($\hat{z}$), and the other principal axis is aligned with $\hat{x}$. We choose the TE0 mode, for which $\underline{E}$ for the guided light is directed mainly along $\hat{x}$. The ring is designed to be near-critically coupled to the bus waveguide when the SnSe ZZ axis is aligned with $\hat{x}$ (ZZ $\parallel \hat{x}$). When the ferroelastic domain is switched, the resonance shifts, providing a means to control the transmission along the bus waveguide. We optimize the length of the SnSe patch and the coupling coefficient (defined as the ratio of electric field amplitudes in the bus waveguide and in the resonator) to optimize the transmission on/off ratio while minimizing insertion loss (SI).

In Figure 2b, we show the transmission spectra for a SnSe patch length of 35 μm; the inset shows the $n(\lambda)$ and $k(\lambda)$ data used in the simulation. The device has a broader linewidth and higher insertion loss for AC $\parallel \hat{x}$. At $\lambda = 1.2615\,\mu m$, the difference in transmission between ZZ $\parallel \hat{x}$ and AC $\parallel \hat{x}$ is 0.74. This large dynamic range suggests the possibility of designing a multilevel device. To simulate such a device, we place a $32 \times 1$ array of monolayer SnSe patches on the waveguide, where each patch has area $1.1 \times 1.2\,\mu m^2$ (Figure 2c). By sequentially switching the patches between ZZ $\parallel \hat{x}$ and AC $\parallel \hat{x}$ configurations, we simulate a device with 32 discrete transmission levels (Figure 2d).

We also simulate devices using bulk (i.e., many-layer thick) SnSe. As for the monolayer case, we use published, theoretically predicted refractive index data.[22] Using this data, we find that bulk SnSe features a FoM of 0.68 at $\lambda = 1.55\,\mu m$, with

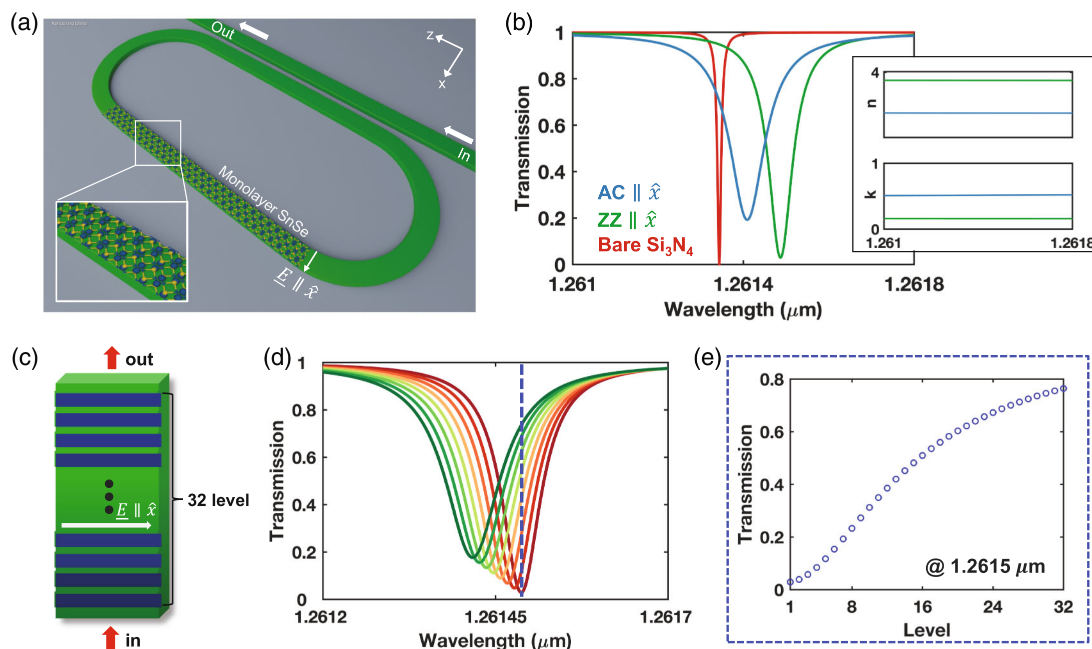


**Figure 2.** Simulating a switchable ring resonator using a monolayer SnSe active layer. a) Device illustration (not to scale). b) Transmission spectra for resonator without SnSe (red), resonator with SnSe ZZ $\parallel \hat{x}$ (green), and SnSe AC $\parallel \hat{x}$ (blue). Simulations are for the TE0 mode with $\underline{E} \parallel \hat{x}$. (Inset) The refractive index data $n(\lambda)$ and $k(\lambda)$ used for the simulation. Data are shown for $\underline{E} \parallel$ ZZ (green) and $\underline{E} \parallel$ AC (blue) and are effectively constant within the simulation window: $n_{AC} = 2.76$, $n_{ZZ} = 3.75$, $k_{AC} = 0.51$, and $n_{ZZ} = 0.16$. c) Schematic illustration (not to scale) of $32 \times 1$ array of monolayer SnSe patches, to simulate a multilevel device. d) Variation in device transmission as the 32 SnSe patches are sequentially switched between ZZ $\parallel \hat{x}$ and AC $\parallel \hat{x}$ configurations. Dark red (far right) represents the case of all 32 patches aligned with ZZ $\parallel \hat{x}$; dark green (far left) represents the case of all 32 patches aligned with AC $\parallel \hat{x}$. e) Transmission at $\lambda = 1.2615\,\mu m$ (indicated in (d) by blue dotted line) as the patches are sequentially switched from ZZ $\parallel \hat{x}$ to AC $\parallel \hat{x}$.


© 2021 The Authors. Advanced Photonics Research published by Wiley-VCH GmbH

$\Delta n = 0.50$ and $\sum k = 0.73$. $\Delta n$ is smaller for bulk than for monolayer SnSe, but the larger interaction volume allows devices with shorter interaction length. In **Figure 3**a, we show the results of a simulated $Si_3N_4$ ring resonator with a bulk SnSe active layer, working the telecommunications C-band ($\lambda \approx$ 1530–1565 μm). The $Si_3N_4$ waveguide has thickness of 0.22 μm and width 1.2 μm, and the SnSe active layer has thickness 10 nm and interaction length of 4 μm. Compared with monolayer SnSe, the larger interaction volume produces a larger shift in the resonance position, but the device also has higher optical loss. Due to the large width of the resonance for of ZZ $\| \hat{x}$, the maximum transmission contrast (found at the local minimum for AC $\| \hat{x}$) is 0.52, which is 30% smaller than the maximum contrast for monolayer SnSe. It is noteworthy that polarization-dependent optical response shows the opposite behavior in monolayer and bulk SnSe, that is, in the monolayer case, AC $\| \hat{x}$ is lossier, but in the bulk case ZZ $\| \hat{x}$ is lossier.

We also design a $1 \times 2$ switch integrated with bulk SnSe, as shown in Figure 3b. The $1 \times 2$ switch relies on the asymmetric coupling between a $Si_3N_4$ ridge waveguide and a bulk SnSe-on-$Si_3N_4$ hybrid waveguide operating in the transverse magnetic-field (TM) mode, for which $\underline{E}$ is parallel with light propagation direction ($\hat{z}$). To optimize the geometry, we simulated the hybrid eigenmode supported by the asymmetrically-coupled waveguides using the frequency-domain finite-element method (SI). The cross-port waveguide is set to be 1 μm wide ($w_1$) and 400 nm tall ($t_1$), and it is fully covered by SnSe with thickness of 40 nm. The bar-port waveguide has a width ($w_2$) of 1.2 μm and a height ($t_2$) of 540 nm and is separated from the cross-port by a 200 nm gap, with a waveguide-to-waveguide coupling length of 20 μm. When the SnSe AC axis is aligned with the direction of light propagation (AC $\| \hat{z}$, ZZ $\| \hat{x}$), the phase-matching condition is satisfied, and light incident from the ridge waveguide couples into the hybrid waveguide (Port 1), leading to the cross-switch state (Figure 3c, top). When the ferroelastic domain switches, the phase-matching condition is altered, leading to the bar-switch state (Figure 3c, bottom). In Figure 3d, we show the contrast between the bar-port and the cross-port, $10(\log(T_2) - \log(T_1))$, where $T_2$ and $T_1$ correspond to the transmitted power at the bar-port and cross-port, respectively. The device shows a large contrast upon ferroelectric domain switching, from −10 to 10 dB, over a large bandwidth. Although this performance is not good enough to completely change the light propagation path, it can be used as an effective modulator.

## 3. Properties of and Devices Based on bP

bP is a widely studied material due to its potential usefulness for electronic and mid-IR photonic applications.[23–25] Here, we simulate a ring resonator and a directional coupler using bulk bP, as we do earlier for SnSe. Like SnSe, the crystal structure of bP is orthorhombic and consists of puckered honeycomb layers with inversion symmetry, with a rectangular in-plane unit cell, as shown in **Figure 4**a. We show in Figure 4b the FoM for bulk bP, determined using the complex refractive index, which we

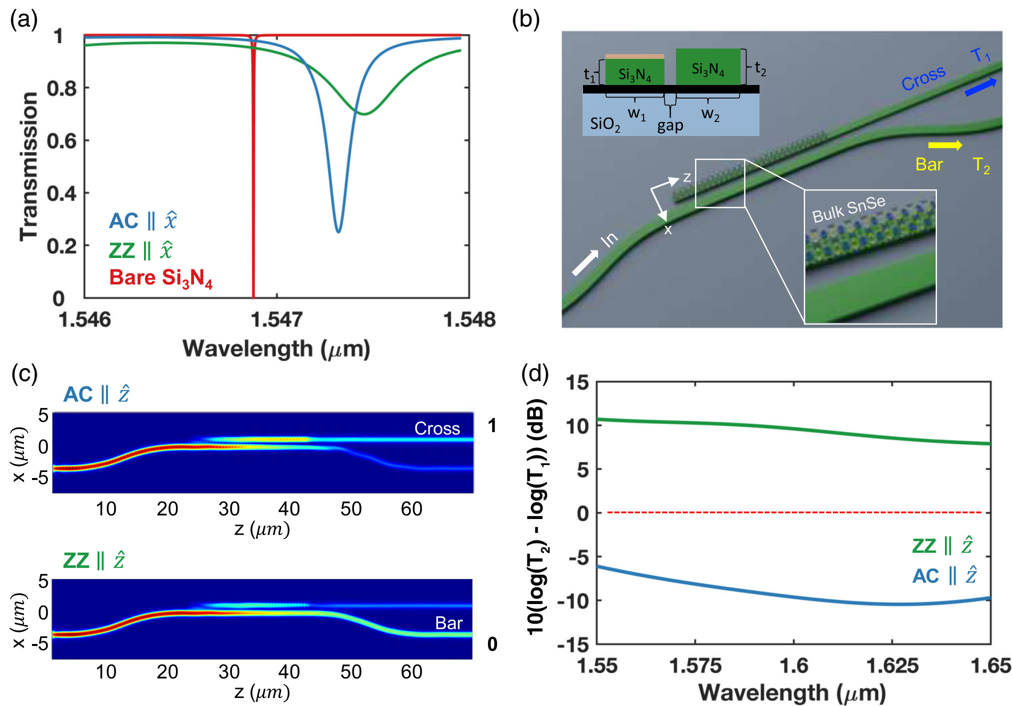


**Figure 3.** Simulating a switchable ring resonator and a $1 \times 2$ switch using a bulk SnSe active layer. a) Transmission spectrum for a bare ring resonator (red), resonator with bulk SnSe with ZZ $\| \hat{x}$ (green), and resonator with AC $\| \hat{x}$ (blue); the geometry is as shown in Figure 2a. b) Schematic of $1 \times 2$ directional coupler. Port 1 is the cross-port and port 2 is the bar-port. The insets show a cross-section view and representation of a waveguide with integrated SnSe (not to scale). c) Representative simulated data at $\lambda = 1600$ nm; the colors indicate optical power. d) The loss contrast between bar-port ($T_2$) and cross-port ($T_1$) for ZZ $\| \hat{z}$ (green) and AC $\| \hat{z}$ (blue).


© 2021 The Authors. Advanced Photonics Research published by Wiley-VCH GmbH

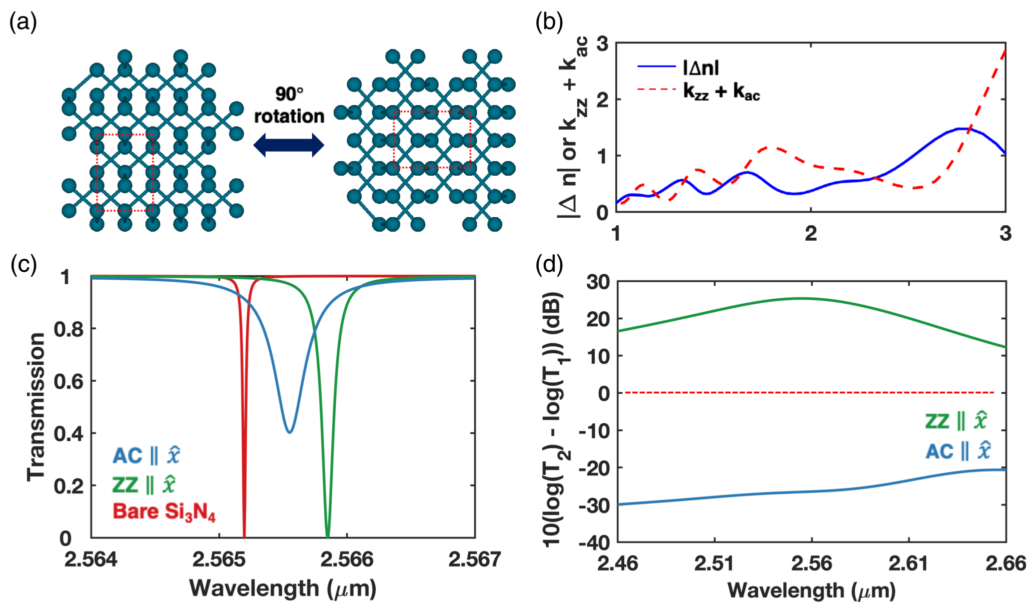


**Figure 4.** Simulating devices based on bP. a) Crystal structure of a single layer of bP, showing ferroelastic domains related by 90° rotation. b) Difference $|\Delta n| = |n_{zz} - n_{ac}|$ and sum $k_{zz} + k_{ac}$ for bulk bP, determined by first-principles calculations. c) Transmission spectrum for a bare ring resonator (red), resonator with bulk bP with ZZ $\parallel \hat{x}$ (green), and resonator with AC $\parallel \hat{x}$ (blue); the geometry is as shown in Figure 2a. d) The loss contrast between bar-port ($T_1$) and cross-port ($T_2$) for ZZ $\parallel \hat{x}$ (green) and AC $\parallel \hat{x}$ (blue) for a $1 \times 2$ directional coupler using bulk bP.

calculate using methods described previously (SI).[26] For bulk bP, a maximum FoM of $\approx 2.5$ is achieved at wavelength $\lambda = 2.58\,\mu$m, at which $|\Delta n| = 1.15$ and $\sum k = 0.45$. Based on this FoM data, we choose to simulate devices operating at $\lambda \approx 2.5\,\mu$m. As noted in Section 1, the theoretical data for bP include a bandgap correction (unlike the theoretical data used for SnSe), and therefore the operating wavelength range simulated here may accurately match future experiments.

We design a ring resonator to be critically coupled to the bus waveguide when the ZZ axis of bP is aligned with the direction of light propagation (AC $\parallel \hat{x}$, as shown in Figure 2a). The resulting device has a $Si_3N_4$ waveguide that is 1.6 μm wide and 330 nm thick, with a bending radius of 100 μm. A bP layer 10 nm thick fully covers the waveguide for interaction length of 5 μm. We show in Figure 4c the device transmission spectrum. The resonance shifts shorter wavelength and develops more optical loss upon switching from ZZ $\parallel \hat{x}$ to AC $\parallel \hat{x}$. This is due to the anisotropy in effective mass: the AC axis has smaller effective mass than the ZZ axis, and as a result bP shows anisotropic plasmonic dispersion.[23] The transmission contrast between the two bP orientations reaches 0.88 at the wavelength of the ZZ $\parallel \hat{x}$ resonance. The on/off ratio is as large as 85 dB, with an insertion loss of 0.53 dB.

We also simulate a $1 \times 2$ switch for the TE0 mode using bulk bP, similar in geometry to that shown in Figure 3b. The $Si_3N_4$ waveguide is 400 nm thick and 2 μm wide, and the bar-port and the cross-port are separated by a gap of 300 nm. Unlike the case shown in Figure 3b, here, both the cross-port and the bar-port are covered with a bP layer of 30 nm thick and 20 μm long. In Figure 4d, we show the contrast $10(\log(T_2) - \log(T_1))$ between the two configurations ZZ $\parallel \hat{x}$ and AC $\parallel \hat{x}$. The device has a switching contrast of $\approx 50$ dB at 2.56 μm; see SI for visualizations of the simulation.

## 4. Conclusion

We have shown that the orientation of the in-plane crystal structure of layered and 2D materials with low symmetry—specifically the triaxial materials SnSe and bP—has a substantial impact on device performance when integrated into photonic integrated ring resonators and $1 \times 2$ switches. Theory predicts that the crystal orientation (i.e., the ferroelastic domain structure) of such materials can be switched through an ultrafast, nonthermal, and low-power method by strong electric fields, due to dielectric anisotropy.[6] Should such predictions be borne out in experiment, then triaxial layered and 2D materials may become quite useful for light-controls-light mechanisms in PICs. Our results may be broadly applicable to layered and 2D materials with ferroelectric and ferroelastic crystal structures, which number more than the two studied here.

## Supporting Information

Supporting Information is available from the Wiley Online Library or from the author.

## Acknowledgements

S.S.J. and C.W. contributed equally to this work. This work was supported by an Office of Naval Research MURI through grant #N00014-17-1-2661 and by the National Science Foundation (NSF) under grant no. 1751736. L.Z. and L.Y. were supported by NSF grant no. 2124934. M.L. acknowledges the University of Washington MRSEC center supported by NSF grant no. 1719797. Computational resources at the Stampede2 supercomputer at the Texas Advanced Computing Center (TACC) were made available with support of the Extreme Science and Engineering Discovery


© 2021 The Authors. Advanced Photonics Research published by Wiley-VCH GmbH

Environment (XSEDE) program, supported by NSF grant no. 1548562. The authors thank Hosung Yoon to help with visualization.

## Conflict of Interest

The authors declare no conflict of interest.

## Data Availability Statement

The data that support the findings of this study are available from the corresponding author upon reasonable request.

## Keywords

black phosphorous, integrated photonic devices, layered materials, tin selenide, triaxial materials

Received: June 17, 2021
Revised: July 29, 2021
Published online: October 7, 2021

[1] A. Singh, S. S. Jo, Y. Li, C. Wu, M. Li, R. Jaramillo, *ACS Photonics* **2020**, *7*, 3270.
[2] H. Yang, H. Jussila, A. Autere, H.-P. Komsa, G. Ye, X. Chen, T. Hasan, Z. Sun, *ACS Photonics* **2017**, *4*, 3023.
[3] G. A. Ermolaev, D. V. Grudinin, Y. V. Stebunov, K. V. Voronin, V. G. Kravets, J. Duan, A. B. Mazitov, G. I. Tselikov, A. Bylinkin, D. I. Yakubovsky, S. M. Novikov, D. G. Baranov, A. Y. Nikitin, I. A. Kruglov, T. Shegai, P. Alonso-González, A. N. Grigorenko, A. V. Arsenin, K. S. Novoselov, V. S. Volkov, *Nat. Commun.* **2021**, *12*, 854.
[4] L. C. Gomes, A. Carvalho, *J. Appl. Phys.* **2020**, *128*, 121101.
[5] M. H. Doha, J. I. Santos Batista, A. F. Rawwagah, J. P. Thompson, A. Fereidouni, K. Watanabe, T. Taniguchi, M. El-Shenawee, H. O. H. Churchill, *J. Appl. Phys.* **2020**, *128*, 063104.
[6] J. Zhou, H. Xu, Y. Li, R. Jaramillo, J. Li, *Nano Lett.* **2018**, *18*, 7794.
[7] H. Xu, J. Zhou, Y. Li, R. Jaramillo, J. Li, *Nano Res.* **2019**, *12*, 2634.
[8] J. Zhou, H. Xu, Y. Shi, J. Li, *Adv. Sci.* **2021**, *8*, 2003832.
[9] G. Shi, E. Kioupakis, *Nano Lett.* **2015**, *15*, 6926.
[10] A. Castellanos-Gomez, *J. Phys. Chem. Lett.* **2015**, *6*, 4280.
[11] M. Gajdoš, K. Hummer, G. Kresse, J. Furthmüller, F. Bechstedt, *Phys. Rev. B* **2006**, *73*, 045112.
[12] S. Saha, T. P. Sinha, A. Mookerjee, *Phys. Rev. B* **2000**, *62*, 8828.
[13] V. Stevanović, K. Hartman, R. Jaramillo, S. Ramanathan, T. Buonassisi, P. Graf, *Appl. Phys. Lett.* **2014**, *104*, 211603.
[14] H.-Y. Song, J.-T. Lü, *Chem. Phys. Lett.* **2018**, *695*, 200.
[15] C. Chowdhury, S. Karmakar, A. Datta, *J. Phys. Chem. C* **2017**, *121*, 7615.
[16] S.-H. Cho, K. Cho, N.-W. Park, S. Park, J.-H. Koh, S.-K. Lee, *Nanoscale Res. Lett.* **2017**, *12*, 373.
[17] C. Wu, H. Yu, S. Lee, R. Peng, I. Takeuchi, M. Li, *Nat. Commun.* **2021**, *12*, 96.
[18] Y. Zhang, J. B. Chou, J. Li, H. Li, Q. Du, A. Yadav, S. Zhou, M. Y. Shalaginov, Z. Fang, H. Zhong, C. Roberts, P. Robinson, B. Bohlin, C. Ríos, H. Lin, M. Kang, T. Gu, J. Warner, V. Liberman, K. Richardson, J. Hu, *Nat. Commun.* **2019**, *10*, 4279.
[19] K. Shportko, S. Kremers, M. Woda, D. Lencer, J. Robertson, M. Wuttig, *Nat. Mater.* **2008**, *7*, 653.
[20] A. Gondarenko, J. S. Levy, M. Lipson, *Opt. Express* **2009**, *17*, 11366.
[21] J. S. Levy, M. A. Foster, A. L. Gaeta, M. Lipson, *Opt. Express* **2011**, *19*, 11415.
[22] J. J. Meléndez, R. L. González-Romero, A. Antonelli, *Comput. Mater. Sci.* **2018**, *152*, 107.
[23] Z. Liu, K. Aydin, *Nano Lett.* **2016**, *16*, 3457.
[24] Q. Guo, A. Pospischil, M. Bhuiyan, H. Jiang, H. Tian, D. Farmer, B. Deng, C. Li, S.-J. Han, H. Wang, Q. Xia, T.-P. Ma, T. Mueller, F. Xia, *Nano Lett.* **2016**, *16*, 4648.
[25] C. Chen, X. Lu, B. Deng, X. Chen, Q. Guo, C. Li, C. Ma, S. Yuan, E. Sung, K. Watanabe, T. Taniguchi, L. Yang, F. Xia, *Sci. Adv.* **2020**, *6*, 6134.
[26] V. Tran, R. Soklaski, Y. Liang, L. Yang, *Phys. Rev. B* **2014**, *89*, 235319.
[27] F. Xiong, X. Zhang, Z. Lin, Y. Chen, *J. Materiom.* **2018**, *4*, 139.
[28] J. Zhou, S. Zhang, *npj 2D Mater. Applic.* **2021**, *5*, 16.
[29] Q. Wei, X. Peng, *Appl. Phys. Lett.* **2014**, *104*, 251915.


© 2021 The Authors. Advanced Photonics Research published by Wiley-VCH GmbH